Numerical simulations of quasi-static and rockfall impact tests of ultra-high strength steel wire-ring nets using Abaqus/Explicit

J.P. Escallón[1] and C. Wendeler[2]

[1]WSL Institute for Snow and Avalanche Research SLF

Flüelastrasse 11 CH-7260 Davos Dorf

juan.escallon@slf.ch

[2]Geobrugg AG Technical Department

Aachstrasse 11 CH-8590 Romanshorn

corinna.wendeler@geobrugg.com

Abstract: Flexible, light-weight wire ring-net barriers are used to stop falling rocks serving as protection for villages and roadways in mountainous regions. The steel wire-ring nets are difficult to model because of their complex geometry. The rings consist of a single steel wire strand wrapped together multiple times, and are connected to one another in a chainmail fashion to form the net. Their geometry and behavior represent a challenge to finite element modeling. This paper presents quasi-static and impact explicit FE simulation results of wire-ring net tests using an approach which relies on the general contact algorithm available in the FE code Abaqus. This approach allows a better description of the physics involved in impact problems related to rock falls. The model accounts for many complex physical processes: high-speed impact, contact with sliding friction, damage initiation and evolution, and strain-rate dependent material behavior. These physical aspects have been taken into account and the parameters involved have been calibrated with real test data. We demonstrate that the modeling approach of the ring net improves the accuracy and predictive value of the simulations.

Keywords: Ultra High Strength (UHS) Steel, Wire-Ring Net, Strain Rate Sensitivity, Rockfall Impact, Mass Scale, Mesoscopic Ring, Macroscopic Ring, Damage, Ductility, Contact.

1. Introduction

Flexible steel wire-net protection systems mainly consist of ultra-high strength steel wire nets supported by steel cables with inelastic brake elements and steel posts. They are used to stop falling rocks in mountain regions in order to protect people and infrastructure. These flexible systems include rockfall canopies (Fig 1a), rockfall fences (Fig. 1b and c), and hybrid structures.

(a) Rockfall canopy

(b) Beckenried rockfall test

(c) 8000 kJ rockfall barrier test in Walenstadt

Figure 1: Rockfall protection systems using flexible wire-ring nets: a deflecting ring net canopy structure supported on steel posts installed at Val d'Anniviers (VS), Switzerland (a), rockfall impact on a flexible wire-ring net fence in Beckenried (NW), Switzerland (b), and rockfall impact test on an 8000 kJ energy dissipation ring net fence in Walenstadt (SG), Switzerland (c).

The wire-ring nets investigated in this paper are used as the intercepting nets of the rockfall protection fences that fulfill European Standards (ETAG027, 2008), and which are able to stop impacts in the range of 5000 kJ to 8000 kJ of kinetic energy (ETAG027, 2008). The highest rockfall energy impact barrier is able to stop a 20 ton boulder with an impact velocity of 28.6 m/s (~ 100 km/h) (see Fig. 1c).

The steel wire-ring net consists of loosely connected wire-rings. The main attribute of the ring net is its loose structure, which allows the rings to vary their positions with respect to each other when the net is loaded. The ring net is therefore very flexible and an optimal configuration of the rings within the net is achieved in response to the rock impact. The rings are made of a single ultra-high strength 3 mm diameter steel wire with n_w windings (n_w = 5, 7, 12 and 19). The investigated rings have a 300 mm internal diameter, and the wire bundle is held together by three ring metal clips (see Fig. 2). The ultra-high strength (UHS) steel alloy used for the fabrication of the investigated ring nets has a minimum yielding strength of 1770 MPa.

(a) UHS steel wire-ring (b) Ring components

Figure 2: Steel wire-rings (a), Components of the rings: single UHS steel wire strand bent nw times and steel clips (b).

The mechanical behavior of these ring nets has been studied by performing quasi-static tensile tests (Gottschang, 2001) and impact tests (Grassl, 2002), which allowed developing a node-based ring net model implemented in the finite element code FARO (Volkwein, 2004). These ring nets have been modeled in LS-dyna (Yiu, 2012) taking into account ring-to-ring contact, an element based ring net, and a macroscopic ring representation of the mesoscopic ring. The macroscopic model considered a single cross section with a single winding. Other types of ring nets used for rockfall protection systems have been experimentally tested and modeled in Abaqus/Explicit using an element based ring net model composed of equivalent trusses (Gentilini, 2012).

The 3 mm diameter UHS steel wire fails at ~ 6% of total strain; however, this is assumed to be due to necking. The total elongation of the UHS steel alloy used for the fabrication of the studied ring nets is assumed to be 11%. In this paper, the onset of damage and the ductile damage behavior are investigated. These aspects are fundamental in order to predict the net behavior after damage initiation. The net behavior after subsequent impact will be affected if damage has taken place. Moreover, the strain-rate sensitivity of steel has been commonly neglected. However, incorporating this behavior into the FEM increases the quality of the simulations.

In this paper the rings are studied adding other physical details, such as strain-rate hardening, sliding friction, damage initiation and evolution, which have broadened the current knowledge of the wire-ring net dynamical behavior. These aspects have been studied using the FE code Abaqus/Explicit 6.12.

2. Experiments

In this section, a brief description of the quasi-static tensile tests performed in the Swiss federal Institute of Technology Zurich ETHZ (Gottschang, 2001), and of the impact tests performed in the Walenstadt (SG, Switzerland) test field (Grassl, 2002) are discussed.

2.1 Quasi-static tensile tests

To study the non-linear behavior of the wire-rings and to determine their deformation capacity, laboratory quasi-static tensile tests were performed. Different configurations of single rings and groups of rings were investigated (see Figure 3). The multi-ring tests were also used to calibrate the sliding friction between the rings.

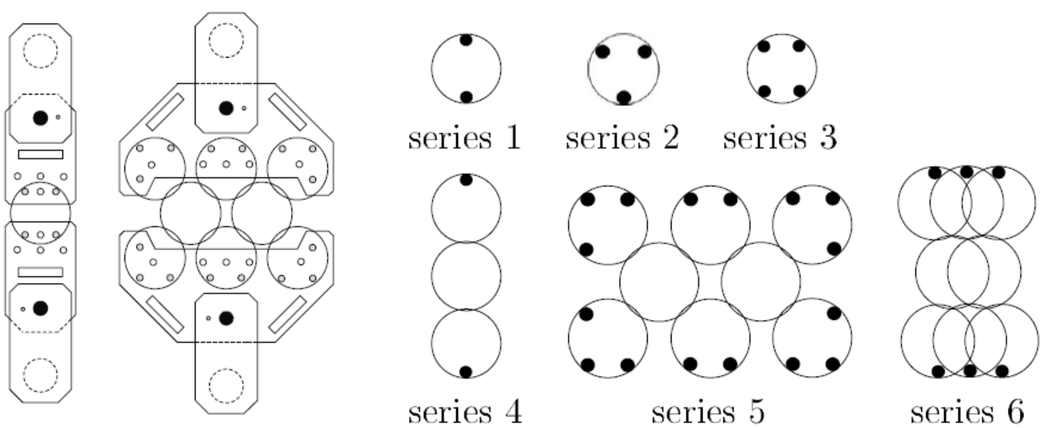

Figure 3: Quasi-static tensile tests with 300 mm diameter steel wire-rings: Test apparatus and overview of tests series (source: Grassl, 2002).

The test laboratory tests were performed using a machine that allows the controlled movement of the upper half of the test apparatus. The lower half of the test frame remains fixed and thus a reaction force can be measured. The different load configurations are explored by using different bolt configurations. The tests were performed under a deformation velocity from 0.1 mm/s to 1 mm/s. In the case of the test series 1, the strain rate can be approximated by the ratio between the bolts displacement and the initial length of the specimen, therefore the strain rates are between $1e^{-4}$ s^{-1} and $1e^{-3}$ s^{-1}. This was observed on the simulations before the stiffness degradation reaches a threshold for which localized high strain rates develop in the small areas subjected to damage.

2.2 Impact tests

In 2002 experimental test series were conducted impacting flexible wire-ring nets either directly fixed to a rigid test frame or attached to flexible cables including brake elements, which are also connected to the rigid test frame. The tests on the net directly fixed to the frame were performed at lower kinetic impact energies (between 24 kJ and 49 kJ). The tests with flexible cables were performed at higher energies (between 24 kJ and 259 kJ) (Grassl, 2002). These series of experiments were conducted using an 825 kg spherical concrete impactor instrumented with eight accelerometers (Schädler, 2004). The low energy tests were carried out dropping the impactor from heights 3 – 6 m, while the boulder was dropped from heights 3 – 16 m for the high energy tests. Using this experimental data the finite element code FARO (Volkwein, 2004) was calibrated. In this paper the first series of the low energy tests is analyzed (see Fig. 4).

Figure 4. Test frame with a single spanned 16 m^2 square ring net with 5, 7, 12 and 19 windings per ring supported in a steel rigid frame: Boulder mass m = 825 kg, and falling heights from 3 m to 6 m (source: Grassl, 2002).

3. The numerical approach

The numerical scheme used in the present paper relies on the general contact algorithm of the Abaqus finite element code. The hard contact behavior was approximated by the penalty contact algorithm in Abaqus. This algorithm approximates contact enforcement using penalty stiffness. It adjusts automatically the normal force – overclosure stiffness, allowing a small amount of penetration.

For the numerical analyses Abaqus/Explicit v. 6.12 has been used. The explicit codes have proved to efficiently solve rockfall impact problems provided the simulated total dynamic response time is only a few orders of magnitude longer than the stability limit (Volkwein, 2004; Gentilini, 2012). Furthermore, explicit codes are also suitable for the simulation of quasi-static tests by properly using the mass-scaling approach (Chung, 1998; Han, 2007).

The explicit codes do not require the assembly of the global stiffness matrix, and the global equilibrium is not checked. This allows the solution to proceed without iterations, and without the requirement of tangent stiffness matrices to be formed (Abaqus Analysis User's Manual). It also simplifies the treatment of contact. The time increments are dictated by the stability limit, which is given in terms of the highest eigenvalue in the FE model. From a conservative point of view, the stable time increment is given by the minimum value from all the elements. Therefore, the stable time increment is proportional to the smallest element size in the numerical domain and inversely proportional to the dilatational wave speed across the element.

The ring net is modeled as a composition of rings which can come into contact with one another as in the real ring net system. The ring is modeled as a macro-equivalent structure with a single winding and a unique cross section. The rings are discretized by linear beam elements. This approach allows the use of the true material data, and therefore a better insight of the ring behavior is possible. Ring-to-ring normal and shear contact forces are taken into account.

The ring net discretization by means of linear beam elements was a result of convergence studies that were carried out for every type of simulation. The simulation times of both quasi-static and impact tests were the same as those from the tests in order to consider correctly the strain rates of the simulations.

Sliding-friction was included in the general contact model. In order to calculate shear stresses at the contact interfaces the isotropic Coulomb friction model with the penalty method was used. The penalty method approximates the ideal no slip (relative sliding) during stick with a stiff elastic behavior. A reduction of the friction coefficient with increasing slip velocity and increased pressure may be assumed for the ring-to-ring contact (Philippon, 2004 and Chowdhury, 2008). The ring-to-ring friction coefficient used for the quasi-static tests was 0.25, and for the impact test was 0.15. Following this approach, more test data can be used to fit a decay law. The impactor – ring net friction used for the impact tests was 0.5.

3.1 Modeling the tensile quasi-static tests

The ring net modeling approach was first used to simulate the series number five of the quasi-static tensile tests. The study of the mechanical behavior of the rings under this series of quasi-static tests, allowed us to perform the verification of the UHS steel mechanical properties and to calibrate the macro ring equivalent parameters. Subsequently, the other series of tests were simulated in order to check a good fit is obtained with the parameters previously calibrated.

The test machine was simply modeled by only considering the bolts which were treated as rigid bodies. The bolts elements were discretized into linear tetrahedral elements, for the purpose of having contact facets interacting with the rings. To minimize penetrations and improve contact resolution the beam elements size considered was slightly smaller than the bolts elements size.

The wire-rings are manufactured using UHS steel with typical steel elastic properties (E=210000 MPa and υ = 0.3). The nominal (engineering) σ_{nom} ultimate stresses and their corresponding nominal strains (engineering) ε_{nom} of the 3 mm diameter wire were supplied by the wire-ring net manufacturer. The true stress σ_{true} – plastic logarithmic strain values were obtained using the corresponding transformations.

The converted laboratory data supplied by the manufacturer and the true stress-true strain values of the AerMet 100 steel alloy (Boyce, 2009) are depicted in Figure 5. These values correspond to quasi-static strain rates. It can be noticed the good match between the manufacturer data and the data reported by (Boyce, 2009). The Von Mises yield criterion was used to model the constitutive behavior of the UHS steel composing the macroscopic model of the rings.

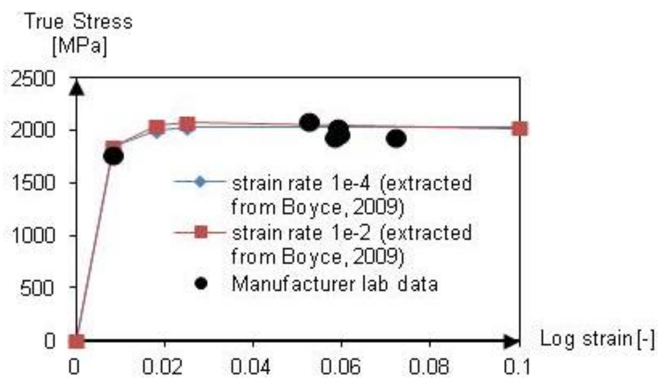

Figure 5. UHS Steel true stress – logarithmic strain data.

The simulation of quasi-static tensile tests allowed us to assess the most important parameters influencing the ring net behavior, particularly, the bending and axial stiffness of the finite beam elements into which the rings are discretized.

The axial stiffness of the beam elements can be expressed as:

$$\mathrm{k_A} = \mathrm{EA_{el}} = E\frac{\pi d_D^2}{4}n_w,$$

where d_D is the single wire diameter; n_w is the number of windings; and E is the steel Young's modulus. The bending stiffness of the beams elements can be expressed as:

$$\mathrm{k_I} = \mathrm{E}\mathbf{I}_{\mathrm{el}},$$

where $\mathbf{I}_{el}$ is the area moment of inertia tensor.

The axial stiffness that can be calculated with a single cross section area equal to the sum of the wire strands areas give a correct measure of the axial stiffness of the wire-ring. However, considering such a cross section overestimates the components of the area moment of inertia tensor, because the area moments of inertia of the mesoscopic wire-ring are smaller than those obtained by considering a full cross section. The chosen approach to deal with this problem in the present paper was to reduce the macroscopic ring cross sectional area to decrease the area moment of inertia tensor; however, this approach leads to an underestimation of the axial stiffness of the ring. In this paper a reasonable compromise between the bending and stretching strength was achieved in order to match the laboratory output curves.

The macroscopic ring equivalent cross-section area A_M is given by:

$$\mathrm{A_M} = \chi \frac{\pi d_D^2}{4} n_w = \chi A_{tot},$$

where χ is reduction coefficient function of the number of windings; and A_{tot} is the sum of the cross section areas of the n_w windings

The area moment of inertia tensor is calculated by Abaqus/CAE based on the simplified geometry considering the macroscopic ring equivalent cross-section area.

These quasi-static tests were carried out using the mass scaling approach. This approach facilitates targeting a predefined time step by increasing the nodal masses. The ratio of the total kinetic energy to the total internal energy was less than 5% over the pulling process, thus maintaining the quasi-static condition.

3.2 Modeling the impact tests

Regarding the simulated impact problem, the slave surface is the ring net surface interacting with the impactor while the master surface is the impactor's surface interacting with the net. For such an experiment the impactor is much stiffer than the net and it behaves as an undeformable body; therefore, the impactor was treated as a rigid body. However, the rigid body was discretized into finite elements with the purpose of having facets to interact with the net. In order to minimize penetrations and improve contact resolution the slave surface in this case is more refined than the master surface. Finally, surface smoothing was used in order to reduce the discretization error associated with faceted representations of curved surfaces.

Since the frame is rigid, deformation takes place exclusively in the wire-ring net. The elements composing it were also treated as rigid bodies, and tie constraints were used to constrain all degrees of freedom. The frame elements are discretized into linear tetrahedral elements, for the purpose of contact with the shackles that attach the net to the frame. Modeling the frame as a rigid body allowed some geometrical simplifications to be made.

The rings as early discussed were discretized by linear beam elements which offer the advantage of taking into account rotational degrees of freedom. This allows the net to deform as observed in the experiments. Out-of-plane behavior can be better modeled with this approach. Ring-to-ring and impactor-to-ring normal and shear contact forces are taken into account.

The steel shackles, which connect the net to the frame, are treated as rigid bodies. The inner rings were discretized by 16 linear beam elements, while the border rings were discretized by 32 linear beam elements to limit the shackle penetration into the rings.

In order to take into account the initial sag of the net due to gravity, a gravity step previous to the test was included. In order to avoid dynamic effects at this step, the gravity was increased smoothly from zero until $g = 9.81\ m/s^2$.

Rate-dependent strain hardening was taken into to model the ultra-high strength steel composing the ring equivalent section. Reported data on UHS steel strain-rate sensitivity (Boyce, 2009) was used to define the set of true stress – true strain constitutive relationships used in the simulations, this data show a 100 MPa increase approximately of the yield stress from a strain rate of $10^{-4}\ s^{-1}$ to a strain rate of $10^{2}\ s^{-1}$. The material data was verified through the simulations. The test for $n_w = 5$ caused damage of some rings which is due to the loss of ductility at strain rates higher than $100\ s^{-1}$. The total elongation estimated for $100\ s^{-1}$ strain rate is 10% approximately. Therefore, a reduction of 1% respect to the quasi-static case is observed. However, the ductility of the steel used to fabricate the rings studied in this paper need to be assessed by laboratory tension tests at the load rates of interest.

In order to avoid the deformation speed to wave speed ratio to increase beyond 0.3 indicating the onset of thermo-mechanical effects, a mass proportional damping α equal to 0.05 was introduced. However, with finer discretization no damping was necessary. Nevertheless, we found no considerable variation in the results when comparing the damped and undamped solutions.

4. Validation of the numerical approach

4.1 Tensile quasi-static tests

The calibrated data from the numerical simulations suggest a linear decay of the reduction coefficient χ with the natural logarithm of n_w (see Fig. 6a). In the last loading stage, ductile damage evolution was taken into account applying a linear damage evolution law in combination with the ductile damage initiation criterion. Abaqus uses Hillerborg's fracture energy proposal (Hillerborg, 1976) in order to alleviate mesh dependency when softening behavior is considered. This is done by creating a stress-displacement response after damage is initiated. The displacement after damage is initiated, or the plastic strain at failure u_f^p was calibrated in order to match the damage behavior observed in the test data. A smooth function approximates the behavior of u_f^p as a function of n_w (see Fig. 6b).

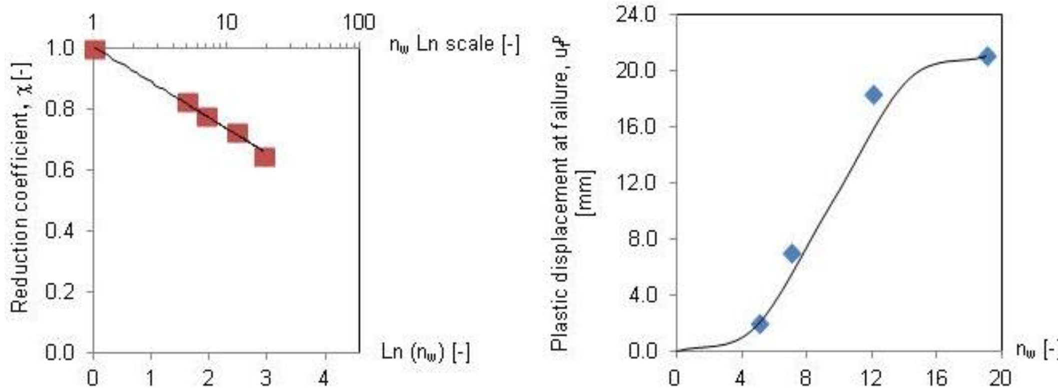

Figure 6. Linear relationship between the reduction coefficient and the logarithmic of n_w (a), linear relationship between the plastic strain at failure ε_f^p and n_w (b).

Therefore, the damage energy which is the integral of the stress-displacement response after damage is initiated also increases following a smooth function as the number of windings n_w increases.

Figure 7a compares the test measurements of the test series 5 for $n_w = 7$ with the simulation results. Figure 7b summarizes the simulation results for all types of rings studied.

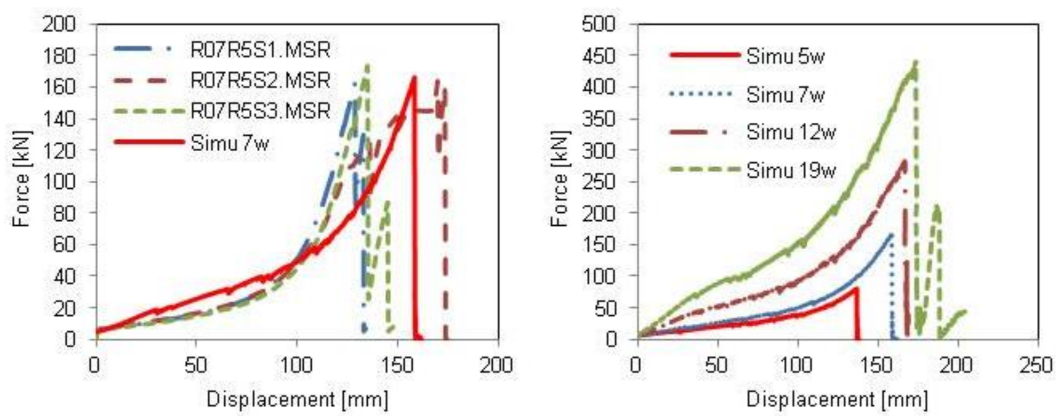

Figure 7. Series 5 test and numerical results for $n_w = 7$ (a), and summary of the simulation results of the 4 types of ring nets studied (b).

The assessment of the test data and simulation results allowed us to understand the ring behavior. The analyzed data indicates that the ring is initially bending and stretching elastically (a). Subsequently, plasticization of the contact zones takes place, and the ring is subjected to elastic-plastic bending and stretching (b). As a consequence, the single wires start to reorder in the cross-section until curvature in the contact zones reaches the maximum (c). Then, the ring undergoes purely stretching and progressive damage takes place at the contact zones (d) (see Fig. 8).

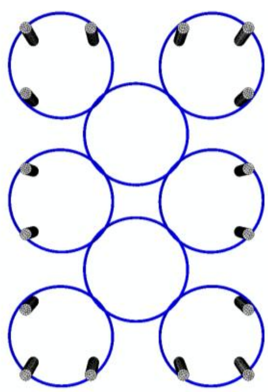

(a) Elastic bending - stretching

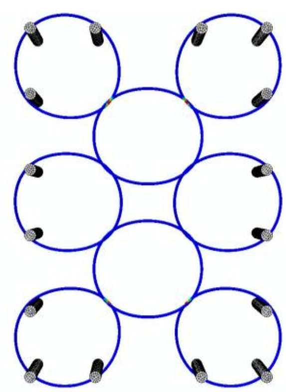

(b) Onset of plastic strains

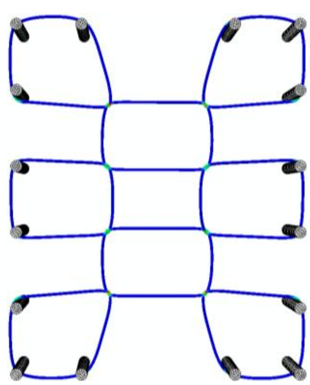

(c) Maximum curvature reached

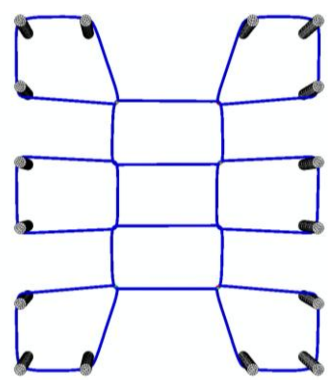

(d) Onset and damage evolution

Figure 8. Pull-out simulation results: (a) elastic bending – stretching, (b) onset of plastic strains at the external ring-to-ring contact zones, (c) maximum curvature is reached at the contact zones, (d) localized damage takes place at the external contact zones.

The simulation results and test data of the series 1 test for $n_w = 12$ are shown in Figure 9. The results show a good match between the test and the simulation data.

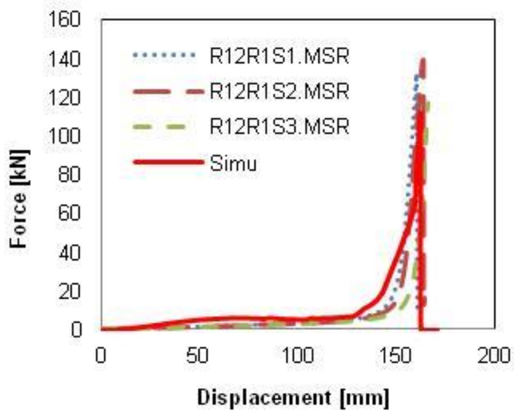

Figure 9. Series 1 test and numerical results for $n_w = 12$.

4.2 Impact tests

Figure 10 demonstrate that the Abaqus/Explicit simulation results in terms of the impactor deceleration/acceleration and velocity show a good match with the test data. Figure 10 shows the simulation results for the case of the wire-ring net with $n_w = 5$.

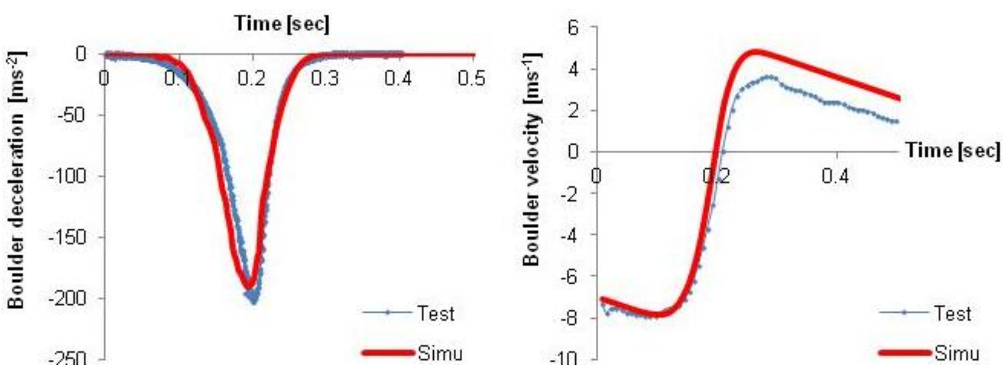

Figure 10. Impact simulation results and test data: (a) boulder deceleration, and (b) boulder velocity for $n_w = 5$.

Figure 11 shows the simulated deformation of the ring net during the 3 m rockfall test. For the sake of clarity the rigid frame and the shackles are not shown.

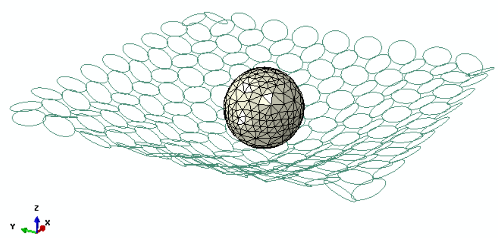

Time elapsed, t = 0 sec

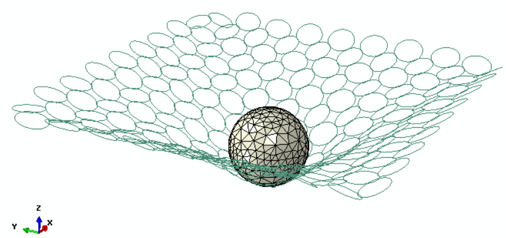

Time elapsed, t = 0.1 sec

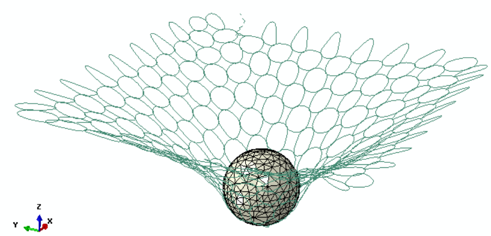

Time elapsed, t = 0.2 sec

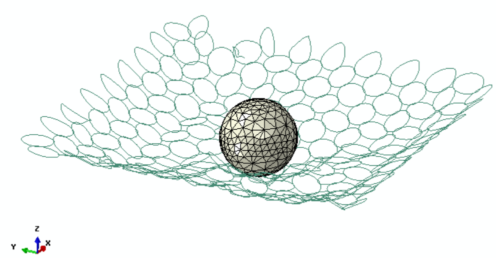

Time elapsed, t = 0.4 sec

Figure 11. Simulated deformation of the ring net during the 3 m drop boulder impact test.

5. Concluding remarks

This paper has presented explicit FEM simulation results of rockfall impact on an UHS steel ring net, taking into account important physical effects such as ductile damage, and strain rate sensitivity. Based on material data reported in the literature and considering the material data supplied by the manufacturer, a set of yielding curves were obtained from a strain rate of 10^{-4} s^{-1} to a strain rate of 10^2 s^{-1}. The material data consider a 100 Mpa increase approximately of the yield stress from a strain rate of 10^{-4} s^{-1} to a strain rate of 10^2 s^{-1}. These yield curves allow a good match of the simulation results with the tests data. Based on the impact simulation results a reduction of ductility of about 1% was considered for strain rates of about 10^2 s^{-1}.

Damage was observed in all quasi-static tests. For $n_w = 5$, damage was also observed in the impact tests. This data allowed the calibration of the ductile damage model available in Abaqus, and the damage behavior observed in the simulations match the damage behavior observed in the tests.

The numerical scheme relies on the general contact algorithm in Abaqus/Explicit. Sliding-friction was included in the general contact model. The applied friction coefficients allow the best match with test data and they are consistent with the sliding velocities.

Mass proportional damping α equal to 0.05 was used. The damping coefficient is sufficiently small to not alter the net deceleration/acceleration behavior but allowed us to avoid the deformation speed to wave speed ratio to increase beyond 0.3 indicating the onset of thermo-mechanical effects.

The reduction coefficient χ allowed decreasing the area moment of inertia tensor components in order to reduce the bending stiffness of the rings without producing a considerable reduction of the tension strength of the macroscopic ring cross section. This coefficient allowed a better match of the force-displacement simulation curves with the test data.

Future tension tests at different load rates such as those carried out by Boyce (2009) on a bar having the same steel alloy used for the fabrication of the studied ring nets are necessary in order to verify the assumptions made regarding material data and to improve the quality of the simulations.

6. References

1. Abaqus Analysis User's Manual, Version 6.12-1, Dassault Systémes Simulia Corp., Providence, RI.
2. Boyce, B.L., and M.F. Dilmore, "The dynamic tensile behavior of tough ultrahigh-strength steels at strain rates from 0.0002 s-1 to 200 s-1," International Journal of Impact Engineering 36 263 – 271, 2009.
3. Chowdhury, M.A., and Md. M. Helali, "The effect of amplitude of vibration on the coefficient of friction for different materials," Science direct, pages 307-314, 2008.
4. Chung, W.J., Cho, J.W., and T. Belytschko, "On the dynamic effects of explicit FEM in sheet metal forming analysis," Engineering Computations, Vol. 15 Iss: 6 pp. 750 – 776, 1998.
5. European Organisation for Technical Approvals. ETAG 27. Guideline for European Technical Approval of Falling Rock Protection Kits. Edition 2008 – 02 -01.
6. Gentilini, C., Govoni. L., de Miranda, S., Gottardi, G and F. Ubertini, "Three- dimensional numerical modelling of falling rock protection barriers," Computers and Geotechnics 44 58 – 72, 2012.
7. Gentilini, C., Gottardi, G., Govoni, L., Mentani, A., and F. Ubertini, "Design of falling rock protection barriers using numerical models," Engineering Structures, 2012 (in press).

8. Gottschang, M., “Trag- und Verformungsverhalten von ROCCO – Drahtringnetzen,” Vertieferarbeit 0909015 Eidgenösisches Institut für Schnee- und Lawinenforschung, 2001.
9. Grassl, H., “Experimentelle und numerische Modellierung des dynamischen Trag- und Verformungsverhaltens von hochflexiblen Schutzsystemen gegen Steinschlag,” DISS. ETH Nr. 14817, 2002.
10. Grassl, H., Volkwein, A., Anderheggen, E., and W. J. Ammann, “Steel-net rockfall protection – experimental and numerical simulation,” Structures under Shock and Impact VII, pp. 143-153, 2002.
11. Han, H., Taheri, F., and N. Pegg, “Quasi-static and dynamic crushing behaviors of aluminum and steel tubes with a cutout,” Thin-Walled Structures 45 283-300, 2007.
12. Hillerborg, A., M. Modeer, and P. E. Petersson, “Analysis of Crack Formation and Crack Growth in Concrete by Means of Fracture Mechanics and Finite Elements,” Cement and Concrete Research, vol. 6, pp. 773–782, 1976.
13. Philippon, S., Sutter, G., and A. Molinari, “An experimental study of friction at high sliding velocities,” Science direct, pages 777-784, 2004.
14. Schädler, S., “Ermittlung dreidimensionaler Starrkörperbewegungen anhand von Beschleunigungsdaten,” Diplomarbeit ETH, 2004.
15. Volkwein, A., “Numerische Simulation von flexiblen Steinschlagschutzsystemen,” PhD. Diss. Swiss Federal Inst. of Technology Zurich, Switzerland, 2004.
16. Yiu, J., Huang, Y., Pappin, J., Sturt, R., Julian, S.H., Kwan and K.S. Ho. Ken, “Landslide Mobility and Flexible Barrier Numerical Modeling Using LS-DYNA,” 12th International LS-DYNA® Users Conference, 2012.

Acknowledgements

The authors thank the CTI for the financial support for this project under the auspices of 12385.1 PFIW-IW. JPE would also like to thank Dr. Perry Bartelt from the WSL Institute for Snow and Avalanche Research, Dr. Axel Reichert from the Dessault Systemes office in Munich, and Prof. E. Chatzi from the Swiss Federal Institute of Technology Zurich for fruitful discussions regarding this topic. The CTI is the commission for technology and innovation of the Swiss Confederation.